Preprint PFC/JA-83-3

RADIATION MEASUREMENTS FROM A RIPPLED-FIELD MAGNETRON (CROSSED-FIELD FEL)

G. Bekefi, R.E. Shefer, and B.D. Nevins

January 1983

RADIATION MEASUREMENTS FROM A RIPPLED-FIELD MAGNETRON (CROSSED-FIELD FEL)

G. Bekefi, R.E. Shefer, and B.D. Nevins

Department of Physics and Research Laboratory of Electronics
Massachusetts Institute of Technology
Cambridge, Massachusetts 02139

Abstract

We report measurements of millimeter wave emission from a rippled-field magnetron (crossed-field FEL). This is a novel source of coherent radiation in which electrons move in quasi-circular orbits under the combined action of a radial electric field, a uniform axial magnetic field and an azimuthally periodic wiggler magnetic field. We observe ∿300kW of RF power in a spectral line whose frequency can be continuously varied from ∿32 to ∿45 GHz by varying the axial magnetic field.

I. Introduction

The rippled-field magnetron[1] (or crossed-field FEL) is a novel source of coherent radiation in the millimeter and submillimeter wavelength ranges. The configuration is a hybrid between a smooth-bore magnetron[2] and a free electron laser.[3] Its similarity to the magnetron lies in the fact that the electrons are subjected to orthogonal electric and magnetic fields causing them to undergo a $\vec{v} = \vec{E}\times\vec{B}/B^2$ drift. Its similarity to the free electron laser comes from the fact that the electrons are also subjected to a spatially periodic wiggler magnetic field $\vec{B}_w$ which imposes upon them an undulatory motion.

The device is illustrated schematically in Fig. 1. It comprises a smooth cylindrical cathode of radius r_c enclosing a smooth coaxial cylindrical anode of radius r_a. The electrons, emitted from the cathode by field emission[2] are subjected simultaneously to two quasi-steady fields acting at right angles to one another: a uniform, axial magnetic field B_{oz} produced by magnetic coils, and a radial electric field $E_{or}(r)$ generated by applying a voltage V between the electrodes. In the absence of the wiggler field, a space-charge cloud forms, partially filling the interaction gap ($r_c - r_a$); the electrons undergo azimuthal rotation having a sheared, radially dependent velocity $v_\theta = E_{or}(r)/B_{oz}$. To achieve this "Brillouin flow equilibrium," the strength of the magnetic field must exceed the critical field for "magnetic insulation", given by[2]

$$B_{oc} = (m_o c/ed_e)(\gamma_o^2 - 1)^{\frac{1}{2}}, \tag{1}$$

where e and m_o are the electron charge and rest mass, respectively, $\gamma_o = 1+(eV/m_oc^2)$ and $d_e = (r_c^2-r_a^2)/2r_a$ is the effective cathode-anode gap width.

Superimposed on the $\vec{E}_o$ and $\vec{B}_o$ fields is an azimuthally periodic magnetic wiggler field $\vec{B}_w$, which perturbs the Brillouin flow of the electron stream. Subject to the requirement that $\nabla\cdot\vec{B}_w = \nabla\times\vec{B}_w = 0$, the field in the vacuum gap between the cathode and anode is calculated to be,

$$\vec{B}_w = \hat{r}\,\frac{B_{ow}}{2}\cos(N\theta)\left[\left(\frac{r}{r_c}\right)^{N-1} + \left(\frac{r_a}{r}\right)^{N+1}\right]\left[\frac{r_c}{r_a}\right]^{(N^2-1)/2N}$$
$$- \hat{\theta}\,\frac{B_{ow}}{2}\sin(N\theta)\left[\left(\frac{r}{r_c}\right)^{N-1} - \left(\frac{r_a}{r}\right)^{N+1}\right]\left[\frac{r_c}{r_a}\right]^{(N^2-1)/2N} \tag{2}$$

where $\hat{r}$ and $\hat{\theta}$ are unit vectors in the radial and azimuthal directions, respectively. $N = \pi(r_c+r_a)/\ell$ is the number of spatial periods and ℓ is the linear periodicity defined midway in the gap. B_{ow} is the amplitude of the radial component of field at a distance $r = r_o \equiv (r_c^{N-1}r_a^{N+1})^{1/(2N)}$ where the azimuthal field component vanishes (which is roughly midway between the cathode and anode). We see that near the center of the gap the wiggler field is primarily radial and is thus transverse to the electron flow velocity $\vec{v} = \vec{E}_o\times\vec{B}_o/B^2$, as is the case in conventional free electron lasers. The undulatory force $-e\vec{v}\times\vec{B}_w$ is along the ±z

axis.

In our device, the wiggler magnetic field is produced by an assembly of samarium-cobalt bar magnets.[4] The placement of the magnets and the electrode configuration are illustrated in the photograph of Fig. 2. The magnets are positioned behind smooth stainless steel electrodes and held in place in grooved aluminum cylinders. Once the system is assembled, the inner electrode (anode) is connected to the positive terminal of the pulsed, high voltage accelerator. The outer field-emission cathode is grounded. Table I gives a summary of the diode dimensions and experimental parameters, and Table II gives data concerning the permanent magnet system.

TABLE I. Summary of operating parameters of the rippled-field magnetron.

Radius of cathode	5.22 cm
Radius of anode	4.43 cm
Length of anode	6.0 cm
Voltage	0.7-1.4 MV
Current	1-20 kA
Pulse length	30 ns
Axial magnetic field	6-15 kG

TABLE II. Summary of the samarium-cobalt bar magnet assembly.

Number of magnets = 96
Dimensions = 0.40×0.40×4.8 cm
Residual induction, B_r = 9.0 kG

Periodicity ℓ (cm)	N	Field Amplitude B_{ow} (kG)
1.26	24	0.68
2.53	12	1.96
5.06	6	2.26

To achieve the different periodicities ℓ given in Table II above, the dipole axes of the magnets are arranged as illustrated in Fig. 3. Because the magnets are discrete, harmonics of the fundamental period $\cos(N\theta)$ are present. However, use of four or eight magnets per period as shown in the second and third diagrams greatly reduces the harmonic content:[4] all even harmonics are absent and the third harmonic also vanishes. As a result, the magnetic field closely resembles that given by Eq. (2). Figure 4 shows a Hall-probe measurement of the radial component of the wiggler field at the center of the cathode-anode gap. Figure 5 gives a computer generated field plot in x,y coordinates. For small gaps such that $(r_c-r_a)\ll r_c$, which is the case in our system, the x,y plot is a good approximation to the actual cylindrical, r,θ, configuration. We see that at the center of the gap, the field is purely transverse (radial); however, at the electrode surfaces, the transverse (radial) and longitudinal (azimuthal) field components are of comparable magnitude. This is of course borne out by Eq. (2).

II. Experiments

Figures 6 and 7 show an overall view of the experimental arrangement. The electric field between cathode and anode is provided by the Physics International Pulserad 110A high voltage facility. The axial magnetic field is generated by two pulsed magnetic field coils surrounding, and coaxial with, the cylindrical electrodes. Typical current-voltage charac-

teristics of the system as a function of the axial magnetic field are shown in Fig. 8. In all cases the magnetic field exceeds the critical field given by Eq. (1).

The radiation generated in the rippled-field magnetron is allowed leak out through the Pyrex window seen in Figs. 6 and 7. We point out that we have as yet not addressed the problem how best to couple out the available radiation. We believe that only a fraction of the radiation generated reaches our externally placed diagnostics. The radiation leaving the Pyrex window in a given direction is received with a horn antenna and rectified in a calibrated crystal detector. To obtain the total emitted power[2] in a given microwave frequency band, we make an angular scan of the radiation pattern of the transmitter, derive its gain and use the familiar radar formula.[2]

The frequency spectra are measured in one of two ways, by means of solid state or waveguide dispersive lines[2] and by a millimeter wave grating spectrometer[5] (shown in Figs. 6 and 7). A dispersive line gives the spectrum in a single firing of the accelerator, but has a rather poor spectral resolution. The grating spectrometer has much better resolution and is used for final, detailed measurements. However, since the spectra must be assembled from successive shots, its use is not practical when the frequency fluctuates, as is sometimes the case. Table III summarizes the frequency bands explored in our studies. However, we shall restrict further discussions to the 26-60GHz range of frequencies because in this range only do we observe a clear narrow spectral line which is unmistakably associated with the presence of the wiggler magnetic field. In the other two bands listed in Table III we observe lower level radiation not clearly connected with the presence or absence of the wiggler. This emission is probably of the same origin as that seen in earlier[2] studies of the smooth-bore magnetron.

TABLE III. Frequency range of spectral studies

Frequency band (GHz)	Method
2 - 4	Solid state dispersive line.
7 - 12	Waveguide dispersive line.
26 - 60	Grating spectrometer; waveguide dispersive line.

Figure 9 shows the total radiated power in the 26-40GHz frequency band, as a function of the axial magnetic field, for a wiggler having a periodicity ℓ=2.53cm(N=12) and an amplitude B_{0w}=1.96kG. The peak emitted power exceeds 300kW. When the wiggler is turned off (by removing the samarium-cobalt magnets from their grooved aluminum cylinders), the emitted power is seen to fall by more than a factor of 20. When the amplitude of the wiggler field is reduced from 1.96kG to 0.98kG (not shown in the figure), the emitted power is reduced by approximately a factor of two. The reduction in B_{0w}, without a change in the period ℓ, is accomplished by removing the azimuthally directed magnets shown in the second diagram of Fig. 3.

Spectral characteristics of the emitted radiation, obtained with the grating spectrometer are illustrated in Fig. 10. The measured line width at the half power points is $\sim$2.2 GHz (the instrument line width is $\sim$1.0GHz). The lower part of Fig. 10 shows that in the absence of the wiggler, the level of radiation has fallen by more than three orders of magnitude; the emission is broad-band and shows no narrow spectral features.

The radiation frequency of the spectral line shown in Fig. 10 varies linearly with the strength of the axial magnetic field. This continuous frequency tuning from 32GHz to 45GHz is illustrated in Fig. 11. At frequencies below $\sim$30GHz (magnetic fields below $\sim$5kG) the emission becomes erratic, probably due to the fact that the corresponding axial magnetic field approaches too closely the critical field of Eq. (1). At frequencies above $\sim$45GHz the amplitude of the spectral line becomes very small. Shot-to-shot reproducibility of the emission is good over the entire frequency range shown in the figure. Thus, detailed grating spectrometer measurements are possible, and these are shown as open circles. The solid dots denote measurements made with a Ka band waveguide dispersive line. The straight line shown in Fig. 11 represents a least squares fit to the experimental data and is of the form,

$$\frac{\omega}{2\pi}\ (\text{GHz}) = 9.4 + 4.0\ B_z(\text{kG}) \qquad \text{for } \ell = 2.53\text{cm} \tag{3}$$

No deterioration of the spectral line profile occurs over the frequency range of Fig. 11; the experimental line width is less than 2GHz.

Changing the period ℓ of the wiggler changes the radiation frequency ω. Figure 12 shows the tuning curve for ℓ=5.06cm(N=6), and a wiggler amplitude B_{0w}=2.26kG. In the measurements the frequency spectra are obtained with the Ka band dispersive line; it appears that shot-to-shot frequency fluctuations prevent use of the grating spectrometer. No line emission occurs at frequencies below ~40GHz. The straight line shown in Fig. 12 is a least squares fit to the data, and is of the form,

$$\frac{\omega}{2\pi}\ (\text{GHz}) = 5.4 + 3.9\ B_z(\text{GHz}) \qquad \text{for } \ell = 5.06\text{cm} \tag{4}$$

It is noteworthy that for a given value of B_z, the radiation frequency is higher for a wiggler of shorter period ℓ, a fact which will be discussed in section III.

III. Discussion

We have observed intense (~300kW), narrow band (≲2GHz) radiation in the millimeter wavelength range (7-9mm). The available radiation is probably much in excess of what we observe. The problem of designing an efficient power extraction circuit has not been addressed yet. Such a design requires better knowledge of the RF mode structure and the physics of the emission mechanism than are presently available.

Dependence of the radiation frequency ω on the externally applied axial magnetic field B_z, and on the wiggler periodicity ℓ suggests that one is dealing with a Doppler upshifted cyclotron mode[6]

$$\omega \simeq (k + k_0)v + \frac{\Omega_c}{\gamma^2} \tag{5}$$

coupled to an electromagnetic wave

$$\omega \simeq kc \tag{6}$$

circulating in the cathode-anode gap. Here ω and k are the radiation frequency and azimuthal wave number, respectively; $k_0=2\pi/\ell$ is the wiggler wave number; v is the azimuthal velocity of an electron interacting with the wave, and $\gamma=(1-(v/c)^2)^{-\frac{1}{2}}$. $\Omega_c=eB_z/m_0$ is the nonrelativistic electron cyclotron frequency associated with the axial magnetic field; and e and m_0 are the electron charge and rest mass, respectively. Eliminating k between Eqs. (5) and (6) yields

$$\omega \simeq (1 + \beta)\beta\gamma^2 k_0 c + (1 + \beta)\Omega_c \tag{7}$$

where $\beta = v/c$.

We see that the empirical Eqs. (3) and (4) have the same structure as Eq. (7). The radiation frequency varies linearly with magnetic field B_z, and for a given B_z, increases with decreasing periodicity ℓ. A quantitative comparison can be made as follows. Determine β by equating the second term of Eq. (7) to the second term of Eqs. (3) or (4). Using this value of β compute the first term of Eq. (7) and compare it with the first term of Eqs. (3) or (4). Table IV summarizes the results.

TABLE IV. Comparison of coefficients a and b in the equation $\omega/2\pi(\text{GHz}) = a + bB_z(\text{kG})$.

	ℓ = 2.53cm β = 0.44	ℓ = 5.06cm β = 0.39
Experiment (Eq. (3) or (4))	$\frac{\omega}{2\pi} = 9.4+4.0B_z$	$\frac{\omega}{2\pi} = 5.4+3.9B_z$
Equation (7)	$\frac{\omega}{2\pi} = 9.4+4.0B_z$	$\frac{\omega}{2\pi} = 3.8+3.9B_z$

There is remarkably good agreement between Eq. (7) and the empirical Eq. (3) for the 2.53cm period wiggler. The agreement is somewhat worse for the 5.06cm wiggler. However, in the latter case, there is fairly large scatter in the experimental data as seen in Fig. 12. We note that the values of β derived above are less than the maximum β that can be imparted by the applied electric and magnetic fields. This implies that only electrons close to the cathode participate in the wave-particle interaction (the velocity $\vec{v} = E_r(r)/B_z$ is sheared; it is zero at the cathode and increases roughly linearly with distance towards the anode). The computed values of β given in Table IV are constant, independent of the strength of the axial magnetic field B_z. This is only possible if the electric field E_r varies such that the ratio $E_r/B_z \simeq$ constant, a fact which is borne out by the voltage versus B_z plot of Fig. 8.

The theoretical understanding of the observed emission mechanism is far from complete, and the validity of Eq. (7) for the radiation frequency must not be overemphasized. Equation (7) is derived[6] under assumptions not really applicable to the experimental device. The single particle computations neglect space charge effects, and the electrons are injected into the cathode-anode gap with finite velocity, rather than being born in situ at the cathode. Finally, the wiggler magnetic field is taken to be purely radial and this neglects the strong azimuthal field component at the cathode and anode surfaces (Eq. (2)). Indeed, with the above theoretical assumptions, the mode represented by Eqs. (5), (6), and (7) is stable, that is, the imaginary part of the complex frequency is zero. We expect to obtain a better understanding of the observed phenomena from a particle simulation code.[7] This is a fully relativistic particle-in-cell code used in previous studies of the relativistic magnetron.[8] Preliminary computer simulations indicate that a large fraction of electrons emitted at the cathode do not in fact circulate but travel directly to the anode. A temporal space charge density modulation occurs accompanied by an azimuthally periodic density variation. An understanding of the emission mechanism will have to take cognizance of the effect of these space charge fields on the dynamics of the circulating component of the electron stream.

An alternate system to the one described above which obviates the undesirable velocity shear present in magnetron-like devices is one in which a monoenergetic electron stream is injected into an azimuthally periodic magnetic wiggler field. This can be accomplished,[9,10] for example, by first passing an annular electron beam of radius r_0 through a magnetic cusp field, thereby transforming the axially flowing beam into an electron ring rotating with an azimuthal speed given by $v=r_0\Omega_c/\gamma$. ($\Omega_c=eB_z/m_0$ is the nonrelativistic cyclotron frequency in the axial guide field downstream from the cusp.) The electrons in the ring then experience an undulatory force $-e\vec{v}\times\vec{B}_w$ in the wiggler field and radiate at a frequency

$$\omega \simeq (1 + \beta)\beta\gamma^2 k_0 c. \tag{8}$$

Such an experiment is in preparation.

Acknowledgements

This work was supported in part by the United States Air Force Office of Scientific Research, and in part by the Department of the Air Force Aeronautical Systems Division (AFSC).

References

1. G. Bekefi, Appl. Phys. Lett. 40, 578 (1982).
2. T.J. Orzechowski and G. Bekefi, Phys. Fluids 22, 978 (1979); and references therein.
3. N.M. Kroll and W.A. McMullin, Phys. Rev. A17, 300 (1978); P. Sprangle and R.A. Smith, Phys. Rev. A21, 293 (1980)
4. K. Halbach, Lawrence Berkeley Laboratory, University of California Accelerator and Fusion Research Division Report No. LBL11393, August 1980.
5. J.A. Pasour and S.P. Schlesinger, Rev. Scient. Instr. 48, 1355 (1977).
6. W.A. McMullin and R.C. Davidson, Bull. Am. Phys. Soc. 27, 1074 (1982).
7. R.D. Estes, A. Palevsky, and A.T. Drobot, Bull. Am. Phys. Soc. 27, 1075 (1982).
8. A. Palevsky, G. Bekefi, and A.T. Drobot, J. Appl. Phys. 52, 4938 (1981).
9. W.W. Destler, P.K. Misra, and M.J. Rhee, Phys. Fluids 18, 1820 (1975).
10. W.W. Destler, R.L. Weiler, and C.D. Striffler, Appl. Phys. Lett. 38, 570 (1981).

Figure Captions

Fig. 1. Schematic diagram of the rippled-field magnetron.

Fig. 2. Photograph of the disassembled rippled-field magnetron, with a samarium-cobalt bar magnet shown in the foreground.

Fig. 3. Arrangement of bar magnets for three different periodicities ℓ.

Fig. 4. X-Y recorder output of the radial magnetic field midway in the cathode-anode gap, as a function of azimuthal angle θ.

Fig. 5. Computer generated magnetic field plot in the cathode-anode gap of a planar version of the rippled-field magnetron.

Fig. 6. Experimental arrangement.

Fig. 7. Photograph of the experimental arrangement showing the glass output window and axial magnetic field coils of the rippled-field magnetron in the background; and the millimeter-wave grating spectrometer in the foreground.

Fig. 8. Current-voltage characteristics of the rippled-field magnetron as a function of the axial magnetic field (B_w=1.96kG, ℓ=2.53cm).

Fig. 9. Radiated power in the 20-40GHz frequency range as a function of the axial magnetic field.

Fig. 10. Emission spectrum in the presence and absence of the magnetic wiggler as measured with the millimeter-wave grating spectrometer.

Fig. 11. Radiation frequency as a function of axial magnetic field for the ℓ=2.53cm period wiggler (● dispersive line measurements; O grating spectrometer measurements).

Fig. 12. Radiation frequency as a function of axial magnetic field for ℓ=5.06cm period wiggler (● dispersive line measurements).

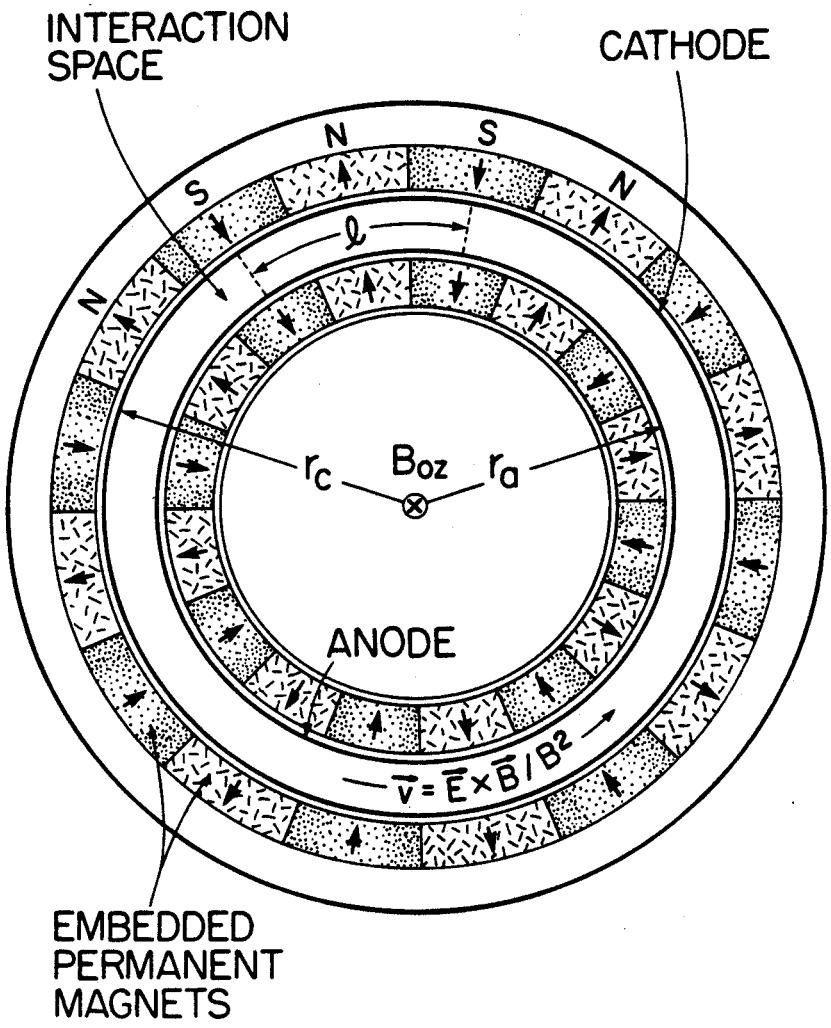

Fig. 1.
Bekefi, Shefer, Nevins

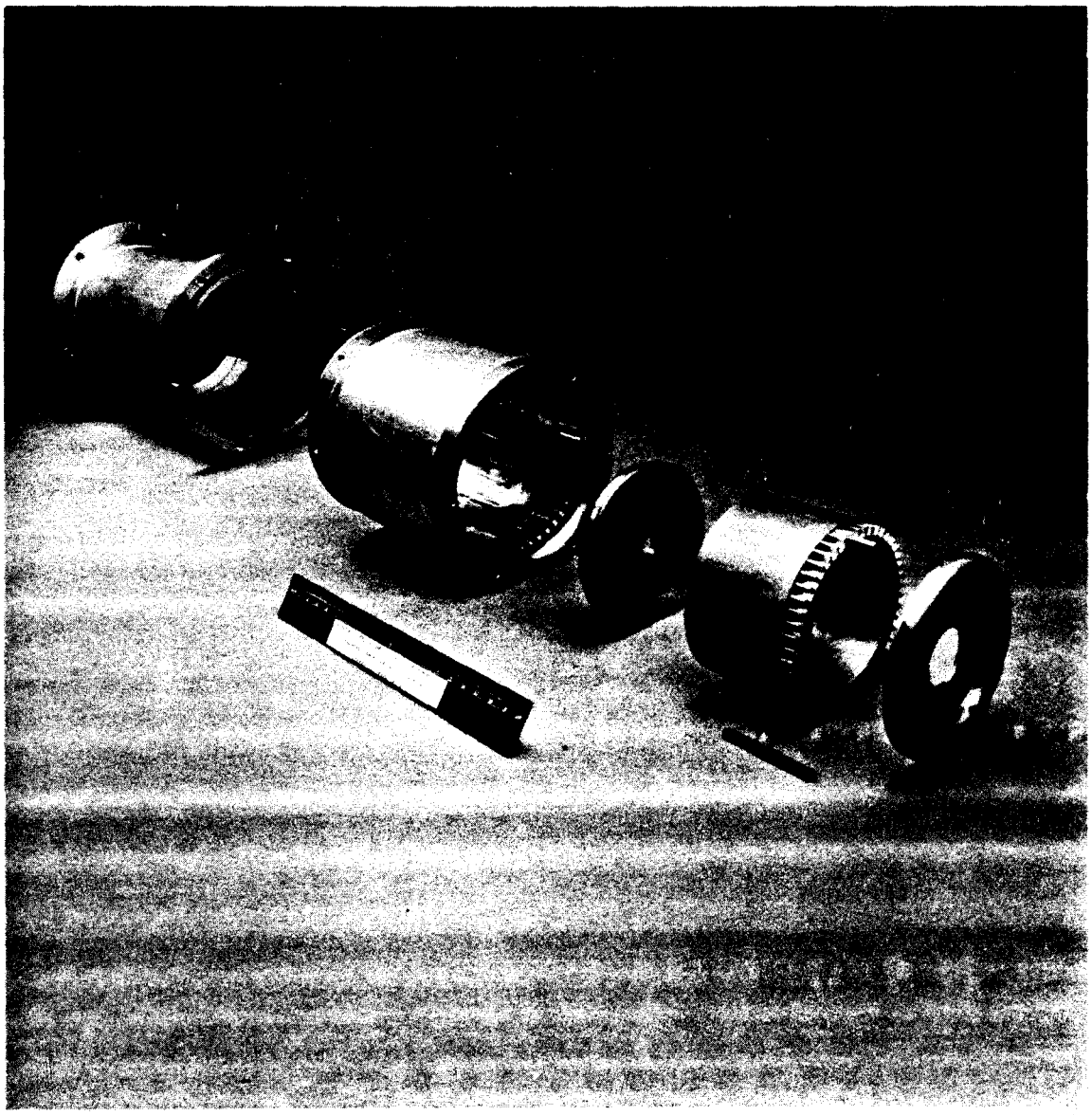

Fig. 2
Bekefi, Shefer, Nevins

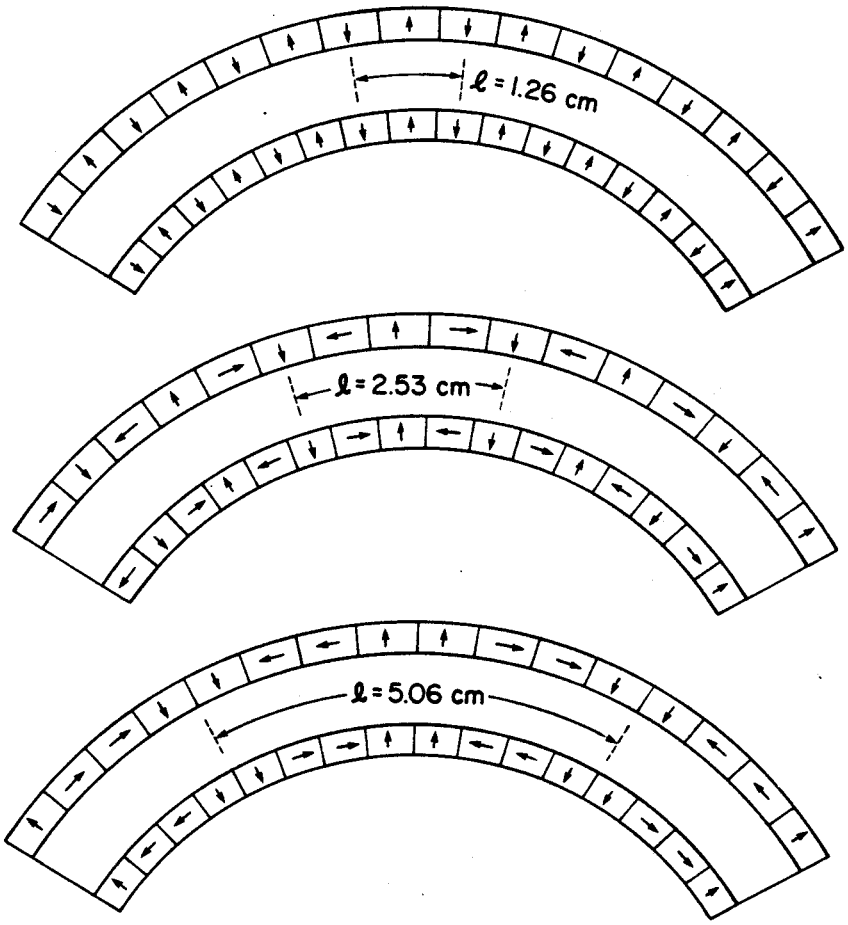

Fig. 3
Bekefi, Shefer, Nevins

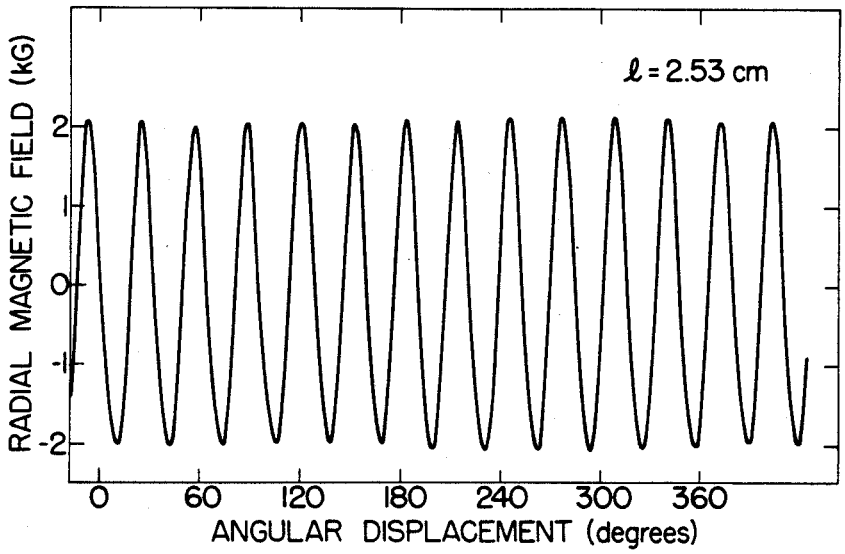

Fig. 4
Bekefi, Shefer, Nevins

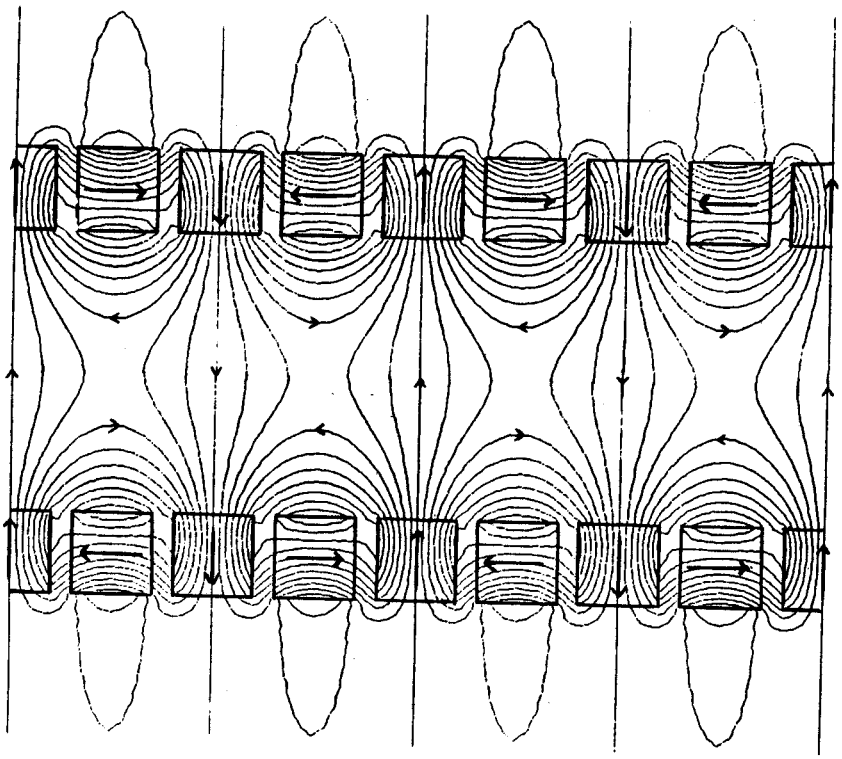

Fig. 5
Bekefi, Shefer, Nevins

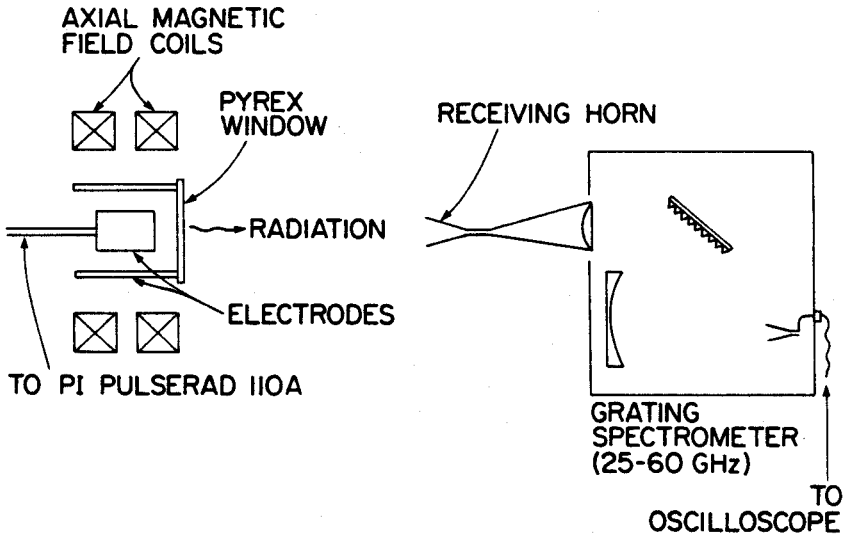

Fig. 6
Bekefi, Shefer, Nevins

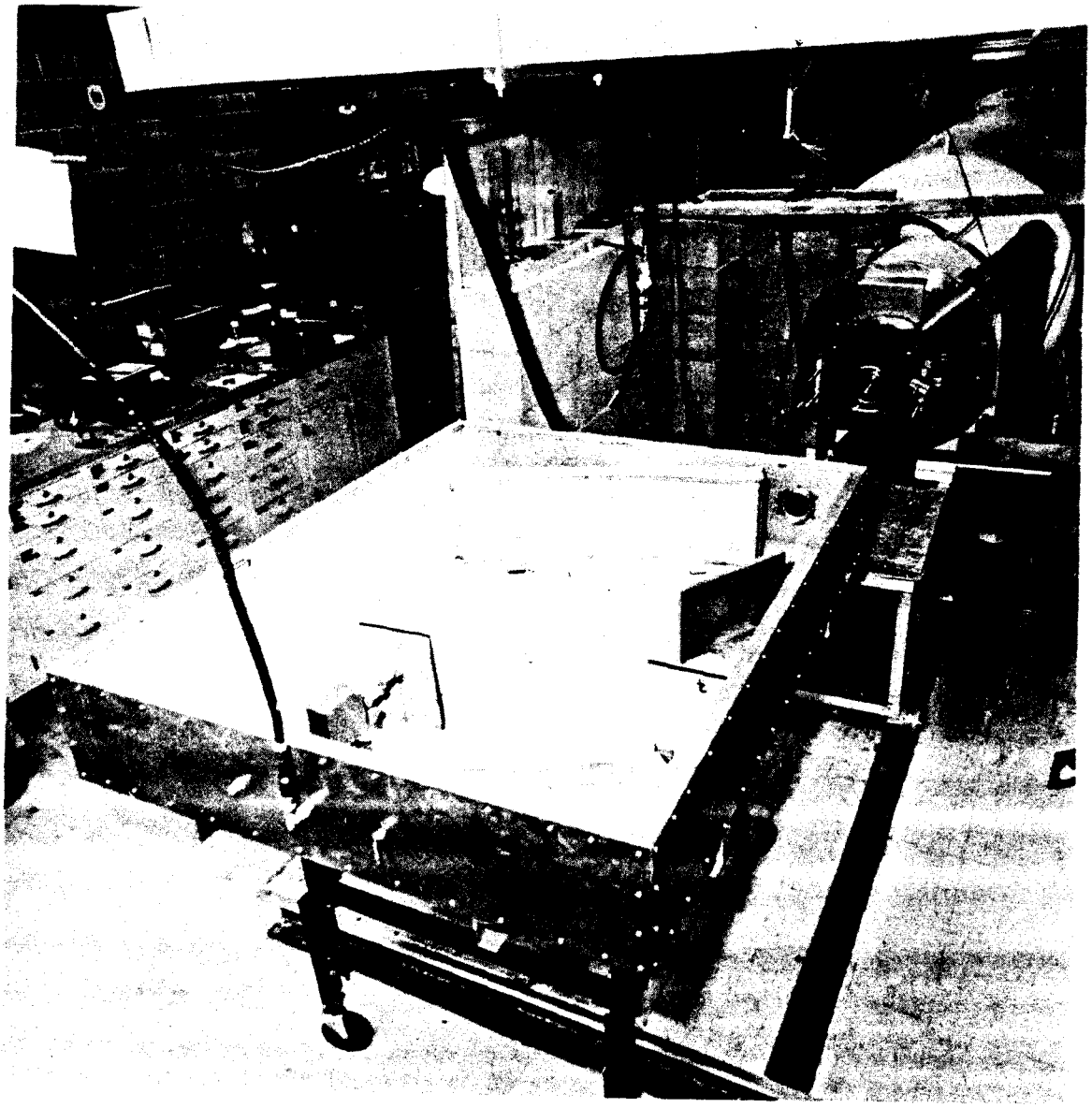

Fig. 7
Bekefi, Shefer, Nevins

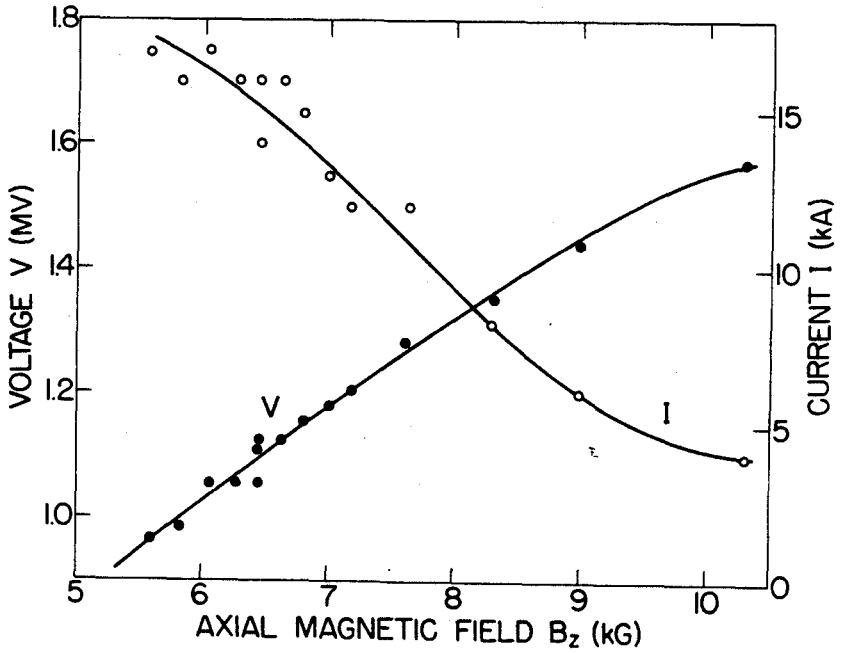

Fig. 8
Bekefi, Shefer, Nevins

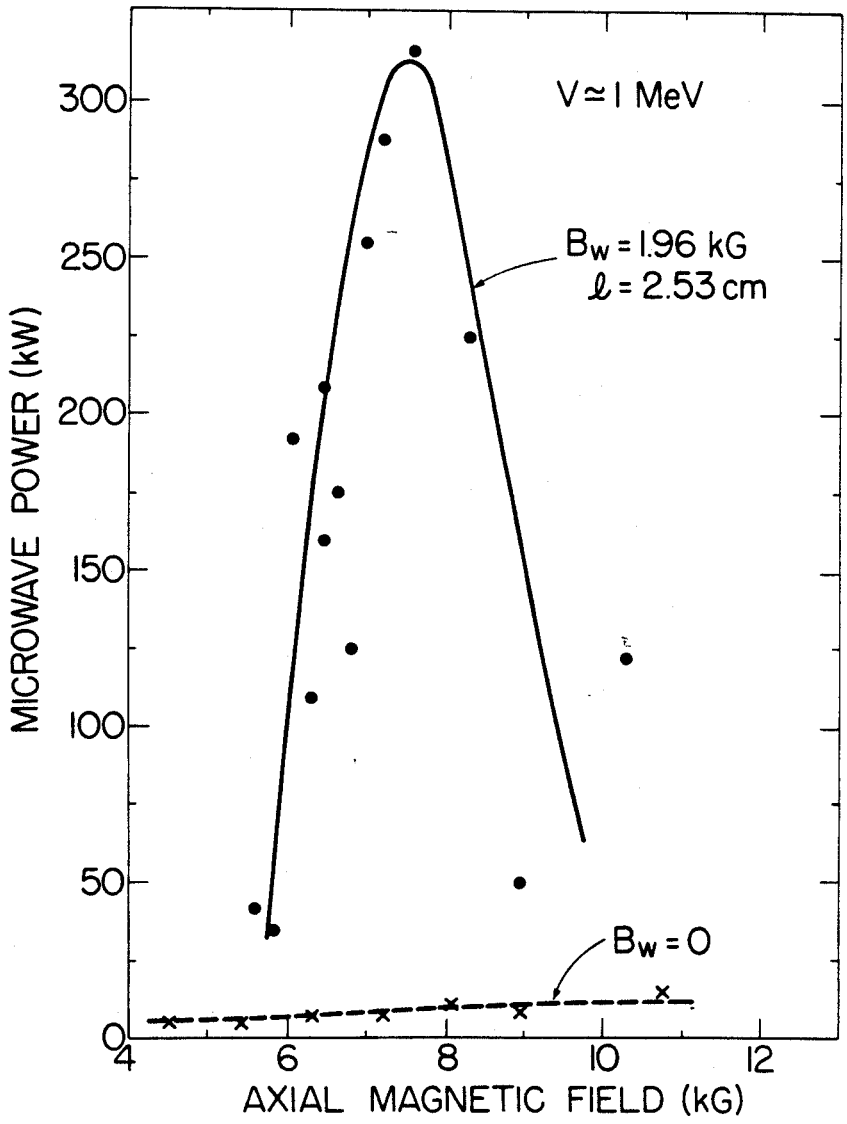

Fig. 9
Bekefi, Shefer, Nevins

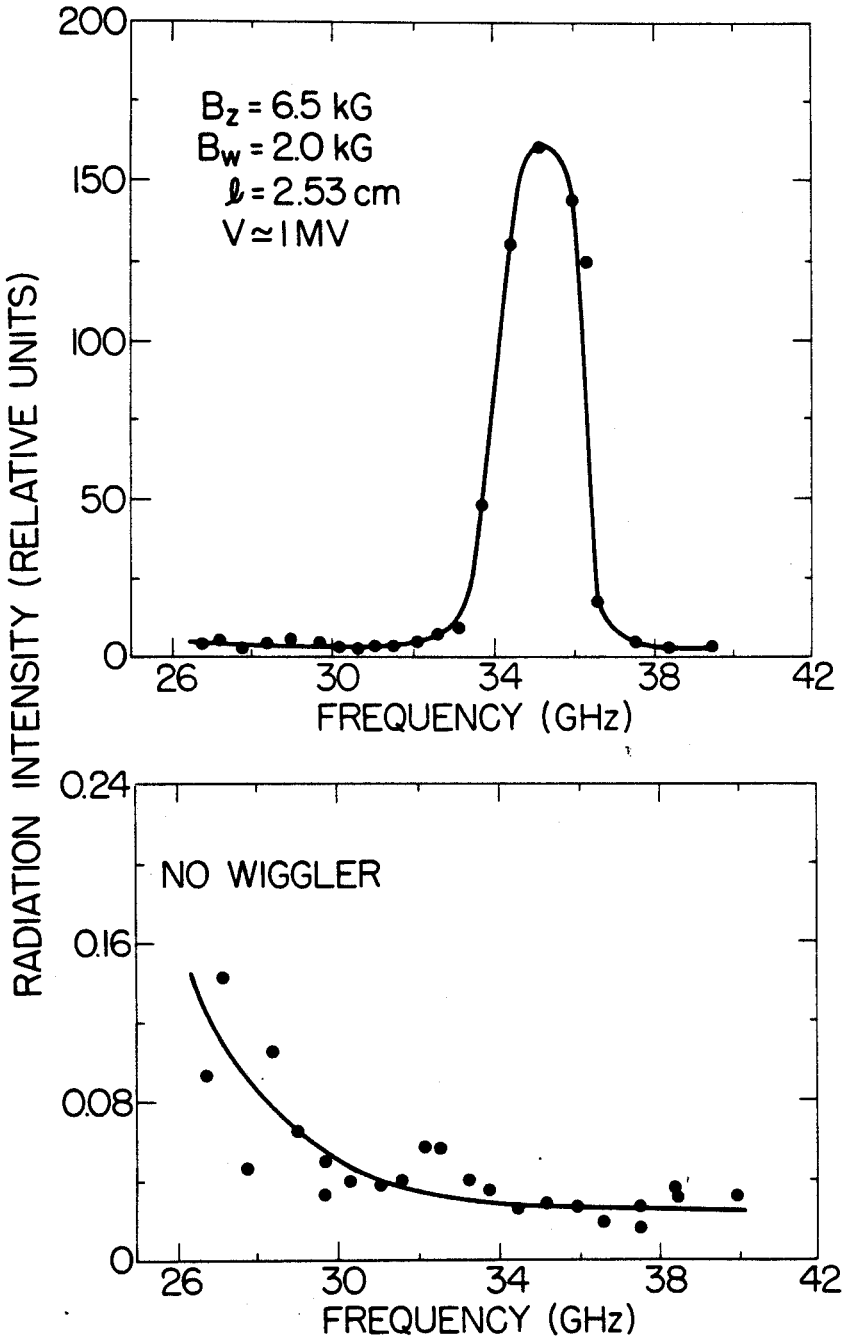

Fig. 10
Bekefi, Shefer, Nevins

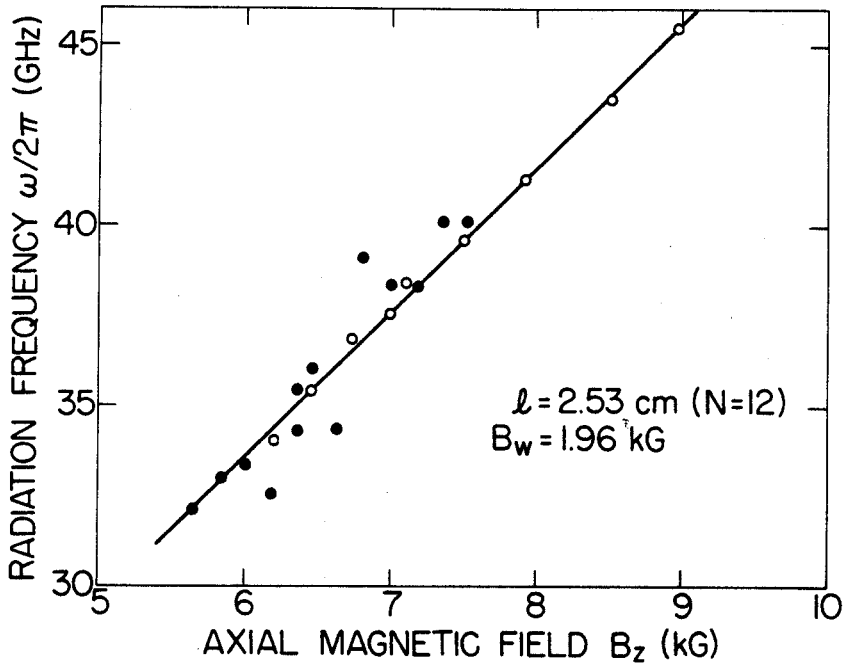

Fig. 11
Bekefi, Shefer, Nevins

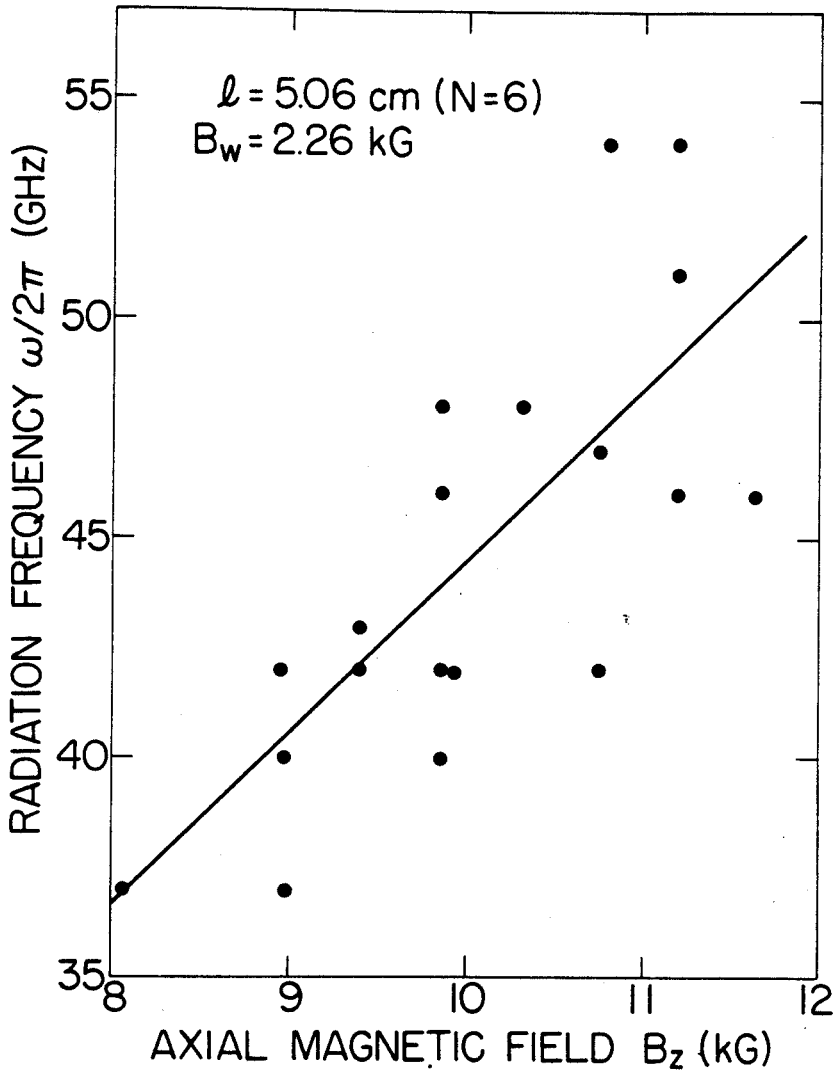

Fig. 12
Bekefi, Shefer, Nevins